Int J Clin Exp Med 2017;10(2):4158-4173
www.ijcem.com /ISSN:1940-5901/IJCEM0043306

Original Article

Silymarin decreases the expression of VEGF-A, iNOS and caspase-3 and preserves the ultrastructure of cardiac cells in doxorubicin induced cardiotoxicity in rats: a possible protective role

Ghalia Mahfouz Attia[1,2], Rasha Ahmed Elmansy[1,3], Sami Awda Algaidi[1]

[1]Department of Anatomy, Faculty of Medicine, Taibahu University, Al Madina Al Monawarrah, Kingdom of Saudi Arabia; [2]Department of Histology and Cell Biology, Faculty of Medicine, Mansoura University, Al Mansoura, Egypt; [3]Department of Anatomy and Embryology, Faculty of Medicine, Ain Shams University, Cairo, Egypt

Received July 22, 2016; Accepted December 2, 2016; Epub February 15, 2017; Published February 28, 2017

Abstract: Doxorubicin (DOX) is the most effective and frequently used anticancer drug. This work aimed to study the protective role of silymarin (SIL) against DOX induced cardiotoxicity. Forty adult male rats were divided into four equal groups; Control, SIL, DOX and SIL-DOX treated groups. Control and SIL groups received daily oral saline (1 ml/kg) and SIL (60 mg/kg), respectively. DOX group received intraperitoneal (IP) injection of 1.66 mg/kg of DOX every second day. SIL-DOX group received the same mentioned doses of both drugs for 12 days. At the end of experiment, blood samples were collected for estimation of serum lactic dehydrogenase (LDH), Creatine phosphokinase (CPK) and aspartate transaminase (AST). Reduced glutathione (GSH) was also estimated. Cardiac specimens were processed for histological, immunohistochemical staining for detection of vascular endothelial growth factor A (VEGF-A), inducible nitric oxid synthase (iNOS), caspase-3 and ultra-structural study. Area percentages of collagen fibers, VEGF, iNOS and caspase-3 immuno expression were measured followed by statistical analysis. Control and SIL groups showed no changes. DOX group showed loss of myofibrils, hemorrhage and congested blood vessels. A highly significant increase in mean area percentage of collagen fibers (23.70 ± 0.44), VEGF-A (27.76 ± 0.57), iNOS (24.002 ± 0.53) and caspase-3 (23.28 ± 0.53) immunoexpression were also detected in DOX group. Mean concentration LDH (326.20 ± 9.908), CPK (233.90 ± 4.581) and AST (97.30 ± 3.112) were increased, whereas GSH was decreased (2.23 ± 0.157). Ultrastructural results revealed loss of myofibrils and intercalated discs and mitochondrial degeneration. These changes were improved in SIL-DOX group. It appears that SIL can protect against DOX-induced cardiotoxicity therefore, could be used in combination with doxorubicin in anticancer therapy.

Keywords: Doxorubicin, cardiotoxicity, silymarin, VEGF, iNOS, caspase-3, ultrastructure

Introduction

Doxorubicin (DOX), also called adriamycin, is the most effective and frequently used anticancer drug of the anthracycline family. It is used in the treatment of several pediatric and adult cancers including leukemia, lymphomas, solid tumors, and breast cancer. However, the utility of doxorubicin is compromised by its severe cumulative cardiotoxicity, including cardiomyopathy and congestive heart failure. Once developed; these cardiotoxic effects carry a bad prognosis and may be fatal [1, 2]. Heart is more susceptible to damage by free radicals because of lower level of protective enzymes compared to other tissues [3, 4]. Other DOX induced toxicities which had been identified in experimental studies include renal [5] and hepatic [6] injuries.

Animal and cell culture model researches couldn't explain the exact mechanism by which DOX induce cardiotoxicity and attributed it to be cellular, molecular, biochemical and genetic. Pre-existing heart disease, extreme age, and radiation therapy have been all suggested to be predisposing factors [7]. However, the wide variation in individual susceptibility to DOX-induced cardiotoxicity cannot be explained by these factors alone. DOX induces cardiac injury by increasing cardiac oxidative stress, leading to activation of inflammation-related signaling

pathway and finally cell death [8]. Recent studies have proved the importance of mitochondrially generated ROS in the regulation of transduction pathways of intracellular signal which help in cell adaptation to stressful conditions and reported the harmful effects of excess production of ROS [9]. Accordingly, approaches aiming at preventing doxorubicin-related toxicities have focused on antioxidants and chelators use to decrease ROS generation.

Silymarin is one of the modern drugs which have been recently used in the alternative and complementary medicine. It is isolated from *Silybum marianum L. Gaertn herb*, which belongs to *Asteraceae family*, one of the largest plant families [10]. It contains mainly silymarin flavonolignans, in addition to small amounts of flavonoids and about 20-35% fatty acids and other polyphenolic compounds. Silybin (also called silibinin) is the main and the major component of the silymarin complex [11, 12]. Silymarin is a known hepatoprotective agent that affects lipid metabolism, stimulates protein synthesis, stabilizes membrane phospholipids and potentiates the physiological antioxidants. It was reported that silymarin can react with ROS and convert them into less toxic and less reactive compounds [13, 14]. Silymarin was also found to decrease the damage to mitochondria and microsomes of rat heart cells by a doxorubicin-Fe^{3+} complex [15]. Moreover, silymarin showed, anti-proliferative, cell cycle - modulating, antimetastatic, antiangiogenic, anti-inflammatory and neuroprotective effects. In addition, a number of experimental models were used to study the antioxidant protective properties of SIL against several toxicants such as Arsenic, Carbon tetrachloride, Thioacetamide and Cisplatinum [16-19].

Therefore, the aim of the present study is to evaluate the possible protective role of silymarin on doxorubicin-induced cardiotoxicity and to correlate between the biochemical, histological, immunohistochemical and ultrastructural changes and their possible underlying mechanism of action.

Materials and methods

Animals

Forty adult male albino rats, 200-250 g were obtained from the animal house of the Medical Research Center, Faculty of Medicine, Ain Shams University. Animals were kept in a good ventilated room and allowed one week for acclimatization at room temperature of 28°C and 12:12 light/dark cycle. Standard rat chow and tap water were provided ad libitum throughout the experiment. The experiment was done according to the regulations of ethical Committee for Animal Experimentation, Faculty of Medicine, Ain Shams University.

Chemicals

1. Doxorubicin was purchased from (D01515, Sigma-Aldrich Chemical Company). It was dissolved in a sterilized 0.9% NaCl solution (2 mg/mL).

2. Silymarin (legalon): Was obtained from Chemical Industries Development Pharmaceutical Co. (CID, Cairo, Egypt) in the form of capsules (140 mg) which were dissolved in sterile water and given by orogastric tube.

Experimental design

The animals were divided into four groups each comprising 10 rats as follows:

I- Control group: Received daily saline (1 ml/kg) by orogastric tube for 12 days.

II- Silymarin (SIL) treated group: Received daily 60 mg/kg by orogastric tube for 12 days with a total SIL cumulative dose 720 mg/kg body weight.

III- Doxorubicin (DOX) treated group: Received intraperitoneal (IP) injection of 1.66 mg/kg of DOX every second day (6 equal doses) during the 12 days of the experiment [12] with a total DOX cumulative dose of 9.96 mg/kg body weight.

IV- Doxorubicin and Silymarin (SIL-DOX) treated group: Received (SIL daily 60 mg/kg orally (12 equal doses) + IP injection of 1.66 mg/kg of DOX every second day for 12 days with a total SIL cumulative dose of 720 mg/kg body weight.

Blood and tissue samples collection

At the end of the experiment, rats of all groups were anesthetized by intraperitoneal injection of sodium thiopental (40 mg/kg of body weight) (Sigma Chemical Co., ST Louis, MO, USA) [20].

In each rat, the thoracic cavity was opened to expose the left ventricle; Blood samples were taken via cardiac puncture and collected in non heparinized tubes for biochemical analysis. The heart was removed and the left ventricle was cut into two halves. One half is chopped into small pieces (1 × 1 mm^2) for preparation of tissue homogenates and electron microscopic study, while the other half was processed for light microscopic examination.

Biochemical study

The obtained blood samples were centrifuged at 3000 r.p.m for 15 min and the sera were used to detect Lactate dehydrogenase (LDH), Creatine phosphokinase (CK) and Asparate amino-transferase (AST). The enzyme activity was measured by a kinetic method using commercial kit (Egyptian company for biotechnology).

Reduced tissue glutathione (GSH)

Small pieces of left ventricles were used for preparation of tissue homogenates, where they were centrifuged at 10,000 rpm for 15 minutes in cold centrifuge. The supernatant was used for estimation of GSH by a colorimetric spectrophotometric method [21] using commercial kits (Bio-diagnostic, Egypt).

Light microscopic study

Specimens of left ventricles were fixed in 10% neutral buffered formalin then washed with water, dehydrated in ascending grades of ethyl alcohol, cleared in xylene, and embedded in paraffin to prepare paraffin blocks which were cut into 5 microns thick pieces. Sections were then mounted on glass slides, deparaffinized in xylene and stained by H&E, Masson trichrome (MT) [22], and immunohistochemical stains for VEGF-A, iNOS and caspase-3 immunoexpression in cardiac cells using avidin-biotin-peroxidase complex (ABC) techniques [23].

Staining procedures for immunohistochemistry

Using strept avidin-biotin technique; Paraffin sections were deparaffinized in xylene, rehydrated, rinsed in tap water, and embedded in 3% Hydrogen peroxide (H_2O_2) in phosphate buffer solution (PBS) for 10 min to block endogenous peroxidase. Sections were incubated overnight at 4°C with the respective primary antibodies. A monoclonal mouse anti-human antibody was used for detection of VEGF-A (Clone No. SP28, Catalog No. M3281, Spring Bioscience, ready to use). Anti iNOS (Ab-1) (Catalog No RB-1605-P0, -P1, Class: IgG rabbit polyclonal; Epitope: Carboxy terminus of iNOS from activated mouse macrophages) (Lab Vision/Neomarkers, Bioanalytica, Greece) was used for detection of iNOS at a dilution of 1:100. A polyclonal rabbit anti-active caspase-3 (Clone No C92-05, Catalog No 55955, PharMingen, San Diego, CA at 1:500 dilution) was used for detection of caspase-3. For detection of VEGF-A and iNOS, an antigen retrieval procedure was applied by pretreatment of sections for 10 min in a microwave oven in 0.01 M sodium citrate buffer (pH 6.0 followed by cooling for further 20 min). Following incubation with primary antibodies, the sections were then incubated with the appropriate secondary antibody; A biotinylated anti-mouse IgG (LSAB™2 Kit; Dako) for VEGF-A and a biotinylated goat anti-rabbit IgG (Vector Laboratories, Burlingame, CA) for caspase-3. Sections were incubated for 30 min at room temperature in horseradish peroxidase-avidin-biotin complex (Vectastain Elite, Vector, CA) then 3,3'-diaminobenzidine in H_2O_2 (DAB kit, Vector, CA), was add to visualize the reaction as a brown, insoluble product. Sections were then counterstained with hematoxylin and mounted. Negative control sections were obtained following the same steps of staining, but without incubation with the primary antibodies.

Electron microscopic study

Specimens for electron microscopy were immediately fixed in 2.5% phosphate-buffered glutaraldehyde solution at 4°C for 24 hours, then washed over night for several times with fresh solution of 0.1 M sodium phosphate buffer, PH 7.4 at 4°C. Thereafter, post-fixed in 2% osmium tetraoxide in 0.1 M sodium phosphate buffer in the dark at + 40°C. Specimens were dehydrated in ascending grades of ethanol and propylene oxide then embedded in resin. Semithin sections were prepared and stained with toluidine blue and examined by light microscope. Ultrathin sections were cut at thickness of 90 nm, mounted on copper grids and stained with Uranyl acetate 5% for 15 min followed by Lead citrate for 8 min and examined by transmission electron microscope SEO (Sumy Electron Optics) model PEM-100 at different magnifica-

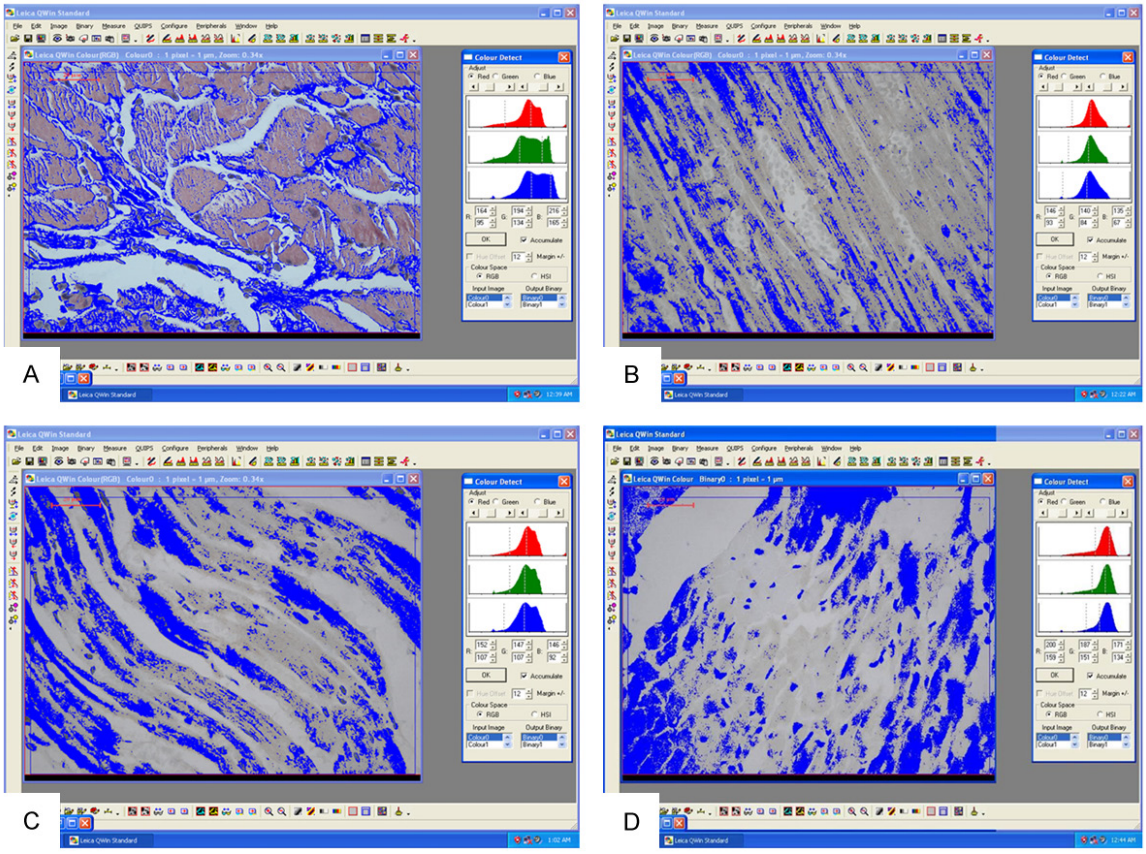

Figure 1. A screen-shot of measurements of (A): Area% of collagen, area% of (B) VEDF (C), iNOS and (D) caspase 3 immunoexpression in DOX group using image analyzer.

tion [24]. Transmission electron examination and photographing were done at Military Medical Academy Electron Microscope Department, Cairo, Egypt.

Morphometric study

Area% of collagen fibers in the cardiac tissue were measured from MT stained sections (× 400) whereas area% of VEGF-A, iNOS and caspase-3 immunoexpression was measured from immunostained section (× 400). Five non-overlapping fields/rat paraffin block sections were examined (The total was 50 measurements/group) and photographed using color video camera (digital camera CH-9435 DFC 290). Photographs of the above mentioned measured parameters were analyzed using Leica Qwin 500 (Imaging System, Cambridge, UK) within a frame area of 293.4288 μm^2. The green color of collagen and the brown color of immunoreaction in the analyzed photos were masked by a blue color as seen in (**Figure 1A-D**). Morphometry was carried out at the Image Analysis Unit, Anatomy Department, Faculty of Medicine, Taibah University, Al Madinah Al Monawarrah, KSA.

Statistical analysis

All data were expressed as mean ± SEM. Statistical analysis was performed using IBM SPSS software version 21.00 (Chicago, Illinois, USA). One-way analysis of variance (ANOVA) (data were normally distributed and variances of populations were equal), *post-hoc* and least significant difference (LSD) were performed for inter-group comparison. $P > 0.05$, $P \leq 0.05$ and $P \leq 0.001$ were considered non-significant, significant and highly significant, respectively [25].

Results

Light microscopic results

H&E stained sections of control and SIL groups showed the same normal general architecture of cardiac tissue, which was formed of bundles

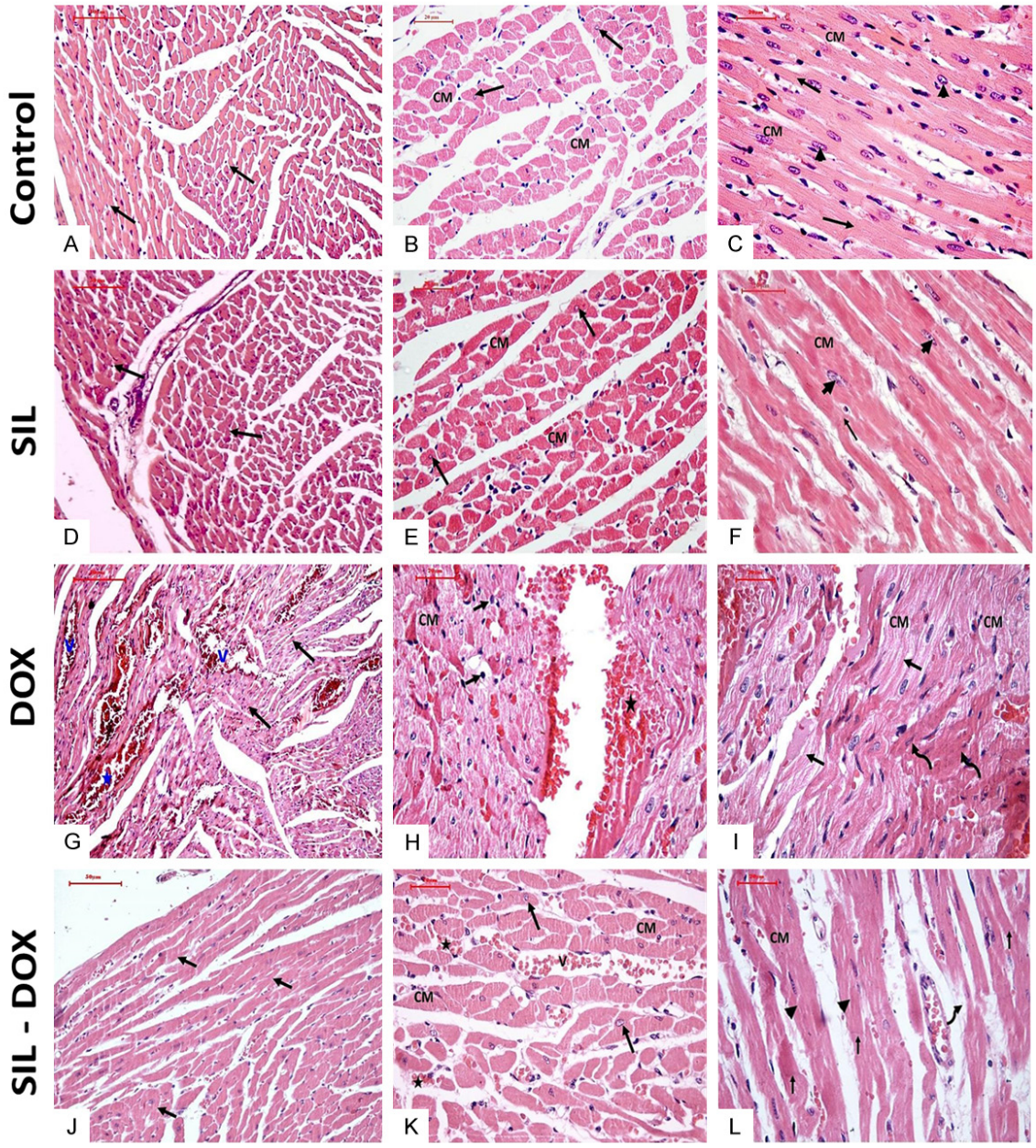

Figure 2. Photomicrographs of heart sections showing: Control (A-C) and SIL (D-F) groups, both have the same normal structure. (A, D) Illustrate the normal general architecture of cardiac tissue which is formed of bundles (arrows) of cardiac myocytes (CM) arranged in different directions. (B, E) Transverse section (TS): CM appear more or less oval in shape with central oval vesicular nuclei (arrows). (C, F) Longitudinal section (LS) of CM showing branching and anastomosing cells with oval nuclei (arrow heads), irregularly striated cytoplasm and the characteristic cardiac intercalated disc (arrows). DOX group (G-I): (G) Show disturbed general cardiac tissue architecture with degenerated CM (arrows), areas of sever hemorrhage (stars) and markedly dilated and congested blood vessels (V). (H) TS of degenerated CM with small deeply stained nuclei. Some cells (arrows) have pyknotic nuclei and vacuolated cytoplasm. Marked hemorrhage (star) is seen between CM bundles. (I) LS showing disturbed, separated and areas of loss of myofibrils (arrows). Cells (curved arrows) with increased eosinophilia and small deeply stained nuclei are also seen. SIL-DOX group (J-L); (J) Nearly normal appearance and arrangement of cardiac cells bundles (arrows). (K) TS of CM with normal shape and appearance and contain vesicular nuclei (arrows). Minimal hemorrhage (star) and minimal congested blood vessels are still seen between the cardiac cells. (L) LS of cardiomyocytes CM showing nearly normal branching and anastomosing cells with central oval vesicular nuclei, normally arranged myofibrils (arrow heads), intercalated discs (arrow). However, few numbers of cardiomyocytes have an area of myofibrils loss (curved arrows). (H&E stain; A, D, G, J: × 200, B, C, E, F, H, I, K, L: × 400).

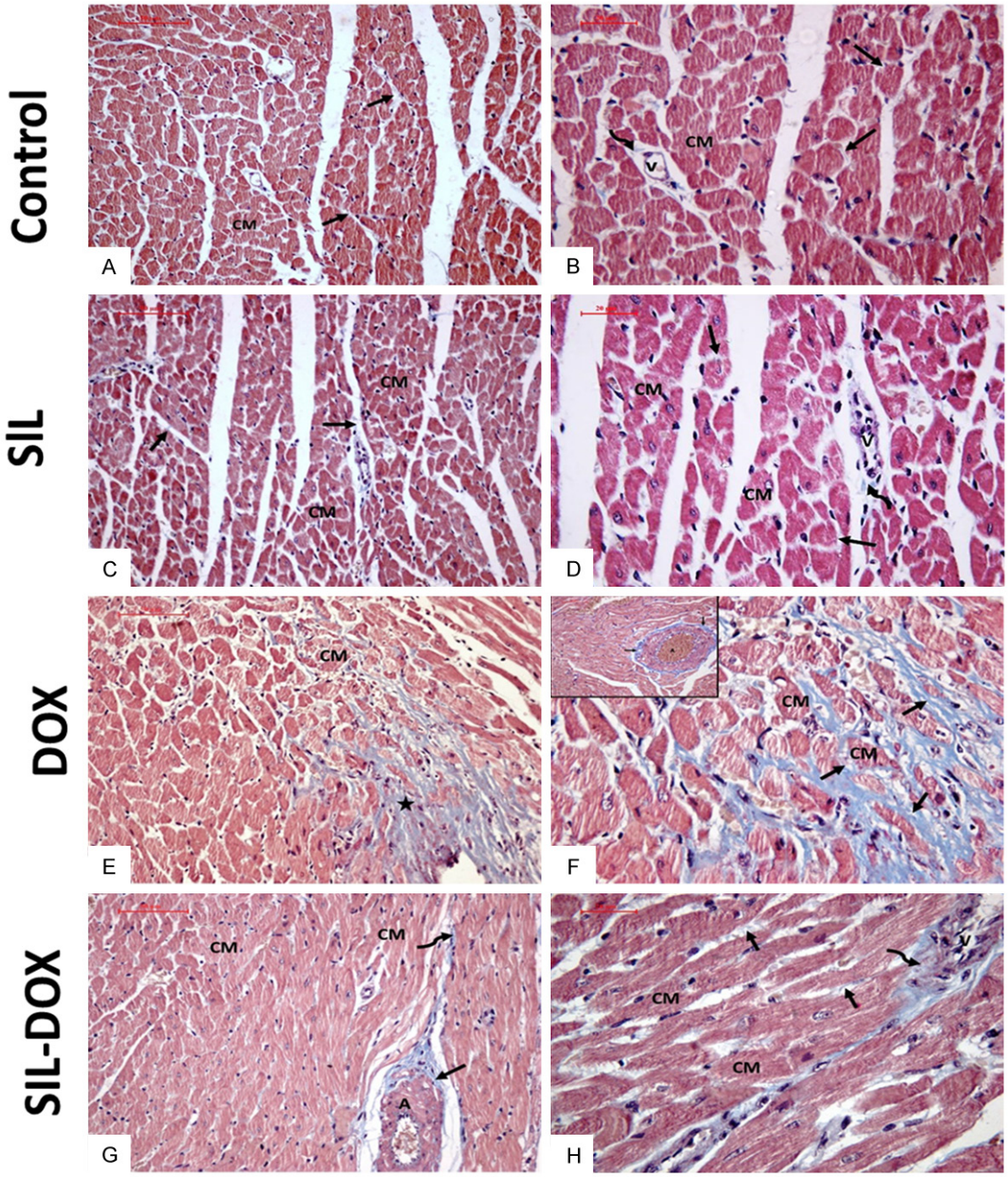

Figure 3. Photomicrographs of heart sections showing: control (A, B) and SIL (C, D) groups. (A, C) Show the same arrangement and distribution of collagen fibers (arrows) between the CM bundles. (B, D) Minimal amount of collagen fibers are deposited mainly around blood vessels (V) and CM (arrows). DOX group (E, F); (E) Show marked increase in the amount of collagen fibers with area of fibrosis (stars) between the CM. (F) Individual CM are markedly surrounded with thick collagen fibers (arrows). Inset show increased amount of collagen (arrows) deposition in the adventitia of coronary artery (A). SIL-DOX group (G, H); (G) Fewer amount of collagen fibers (arrow) between CM and in the wall of the artery (A) are detected when compared to DOX group. (H) CM is surrounded with few amounts of collagen fibers (arrows). Blood vessels (V) show mild condensation of collagen fibers (curved arrow) in their walls. (Masson trichrome stain; A, C, E, G: × 200; B, D, F, H: Inset × 400).

of cardiac myocytes arranged in different directions (**Figure 2A** and **2D**). In transverse sections (TS), cardiac myocytes (CM) appeared more or less oval in shape with central oval

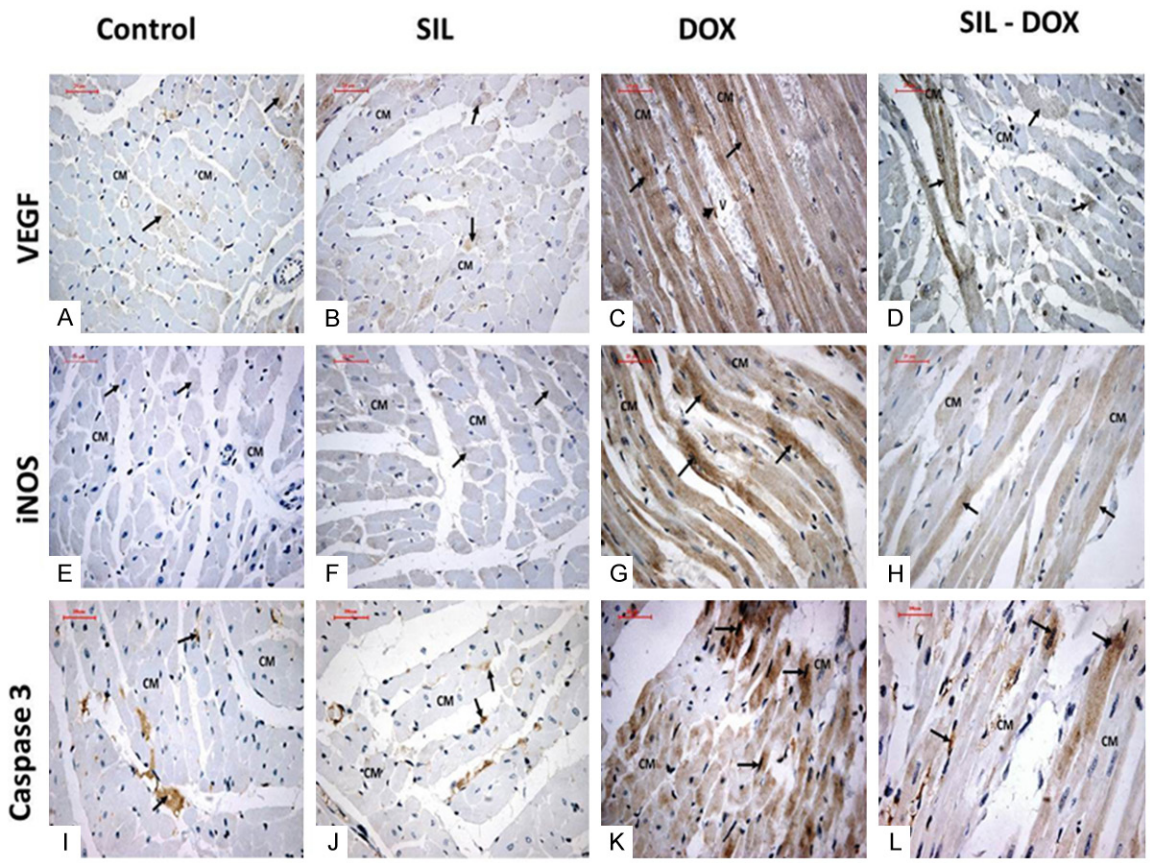

Figure 4. Photomicrographs of immunostained sections of heart showing: VEGF-A immunostained sections (A-D); (A) Control and (B) SIL groups illustrating week VEGF-A (arrows) immunoexpression by CM. (C) DOX group shows strong VEGF-A immunoexpression by most of CM and also in the wall (arrow head) of blood vessels (V). (D) SIL-DOX group: Some CM exhibit mild VEGF-A immunoexpression. iNOS immunostained section (E-H); (E) Control & (F) SIL group, both have faint positive iNOS immunoexpression by CM. (G) DOX group shows CM with cytoplasmic areas (arrows) of strong iNOS immunoexpression. (H) SIL-DOX group: Some CM show mild iNOS immunoexpression (arrows). Caspase 3 immunostained sections (I-L); (I) Control & (J) SIL groups, both show few areas of positive caspase-3 immunoexpression (arrows) in CM. (K) DOX group shows strong nuclear and cytoplasmic caspase-3 immunoexpression (arrows) by CM. (L) SIL-DOX group has mild caspase 3 immunoexpression in CM. (Anti-VEGF-A immunostain; A-D: × 400, Anti-iNOS immunostain I; E-H: × 400, Anti-Caspase-3 immunostain; I-L: × 400).

vesicular nuclei (**Figure 2B** and **2E**). Longitudinal sections (LS) showed branching and anastomosing of CM with oval nuclei, irregularly striated cytoplasm and the characteristic intercalated disc (**Figure 2C** and **2F**). DOX group showed disturbed general architecture with degenerated CM, areas of severe hemorrhage and markedly congested blood vessels (**Figure 2G**). TS revealed degenerated CM with small deeply stained pyknotic nuclei and vacuolated cytoplasm. Marked hemorrhage was seen between CM bundles (**Figure 2H**). Also, CM showed areas of separated and lost myofibrils. Cells with increased eosinophilia and small deeply stained nuclei were also seen (**Figure 2I**). In SIL-DOX group, normal appearance and arrangement of CM were observed, however minimal hemorrhage and minimally congested blood vessels were still seen in between them (**Figure 2K** and **2J**). Normal branching and anastomosing CM with central oval vesicular nuclei, normally arranged myofibrils and intercalated discs were seen. However, few number of CM showed an area of myofibrillar loss (**Figure 2L**).

Masson trichrome stained sections of control and SIL groups showed the same arrangement and distribution of collagen fibers between the bundles of CM (**Figure 3A** and **3C**). Minimal amount of collagen fibers were deposited mainly around the blood vessels and CM (**Figure 3B** and **3D**). DOX group showed marked increase in

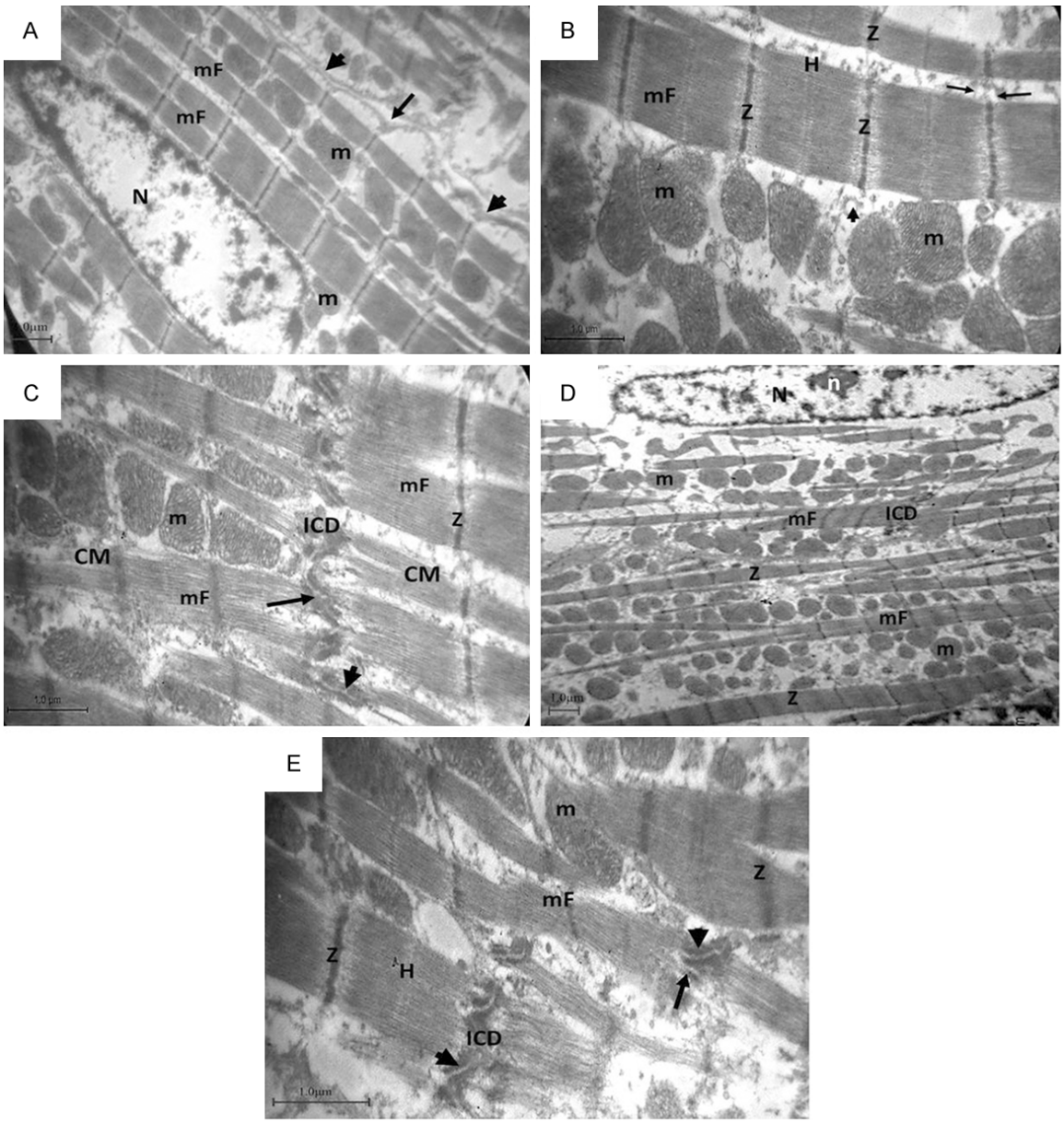

Figure 5. Electron photomicrographs of heart sections from control (A-C) and SIL group (D&E) showing: (A) Control cardiomyocyte with regular arrangement of the myofibrils (mF) which show sarcomers marked by Z lines (Z) in addition to mitochondria (m), rod shaped nucleus (N) with euchromatin, intact regular sarcolemma (arrow heads) and sites of transverse tubules (arrow). (B) Myofibirils with sarcomeres showing Z lines and H zone. Mitochondria (m) with prominent cristae, sarcoplasmic reticulum (arrows) and transverse tubule (arrow head) are also seen. (C) Two cardiomyocytes (CM) are joined together by step like intercalated disc (ICD) which shows fascia adherence (arrow) and desmosomes (arrow head), mitochondria (m) and Z lines (Z) along fibrils. (D) SIL group show cardiomyocyte with rod shaped nucleus (N) with euchromatin, branching and anastomosing myofibrils (mF), which show sarcomeres, regular Zlines (Z) and regularly arranged mitochondria (m) in between the fibrils. (E) SIL group illustrating intercalated disc joining cardiomyocytes together that show fascia adherence (arrow heads) and desmosomes (arrow). Z lines (Z) and H zone (H) are seen along the myofibrils (mF). (TEM; Bar 1 µm, A: × 8000, B, C, E: × 15000, D: × 4000).

the amount of collagen fibers with areas of fibrosis between CM (**Figure 3E**). The individual CM was markedly surrounded with thick collagen fibers. The wall of the coronary artery was also thickened by the increased amount of collagen deposition in its adventitia (**Figure 3F**). In SIL-DOX group, fewer amounts of collagen fibers were detected between CM bundles and in the wall of the artery when compared to DOX group (**Figure 3G**). Blood vessels showed mild

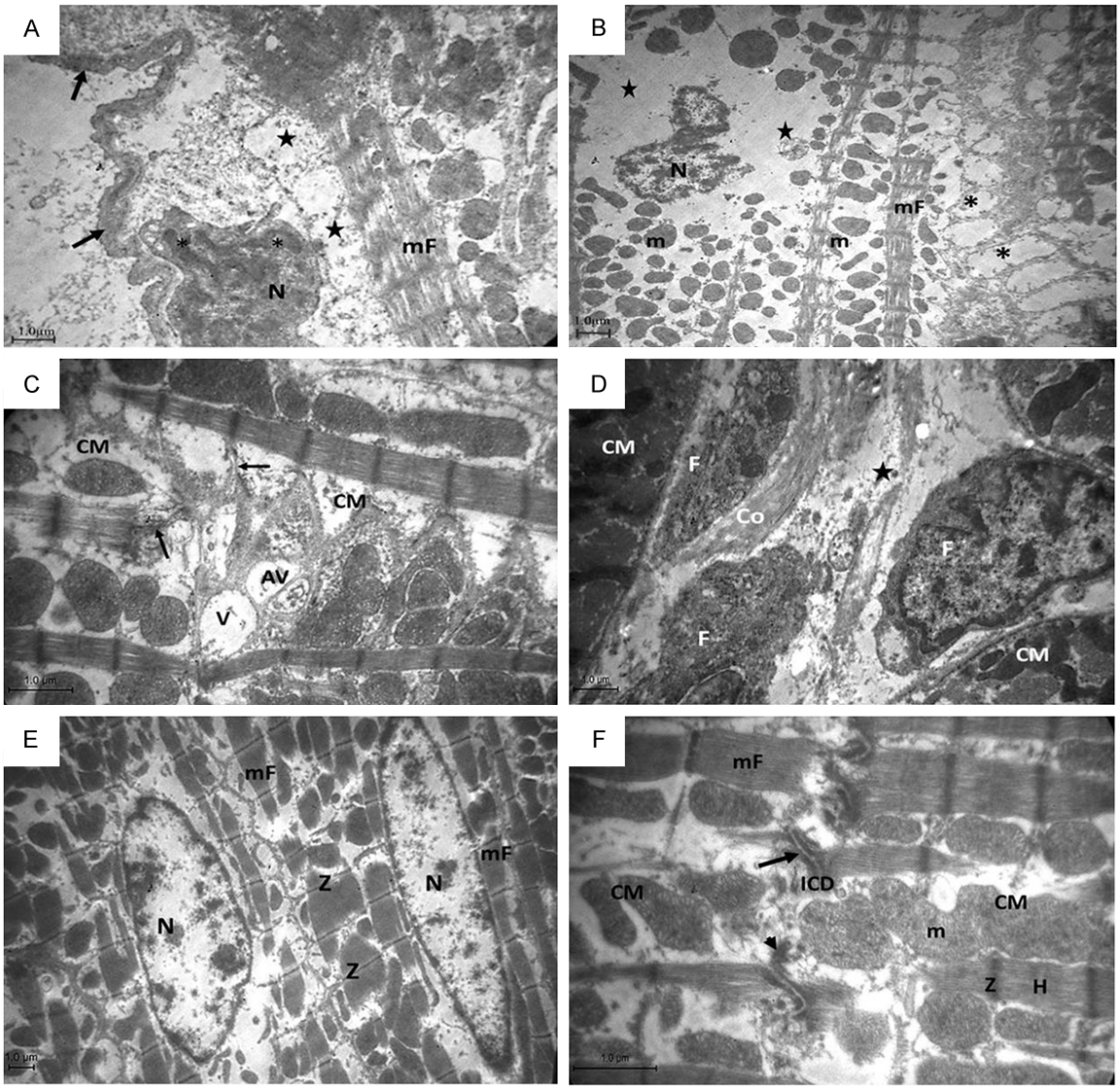

Figure 6. Electron micrographs from heart sections of DOX (A-D) and SIL-DOX groups (E, F) showing: (A) Degenerated Cardiomyocyte with irregular corrugated thick basement membrane (arrows), irregular shaped small peripheral nucleus (N) with peripheral condensation of its chromatin (*), areas of loss of myofibrils in the cytoplasm (stars) and thin irregular nearly lost myofibrils (mF). (B) Degenerated cardiomyocte with small shrunked and fragmenrted nucleus,wide spaces in the cytoplasm (stars), irregular shape and arrangement of mitochondria (m) in between remnants of myofibrils (mF). (C) DOX group showing two cardiomyocte (CM) with lost intercalated disc,except some remnants (arrows), cytoplasmic vacuoles (V) and autophagic vacuoles (Av). (D) Three transversely cut cardiomyocytes with wide intercellular space (star) between them which contain many fibroblasts (F) and collagen fiers (Co). (E) SIL-DOX group show nearly normal appearance of cardiomyocytes with rode shaped nuclei (N) with fine chromatin, regularly arranged myofibrils which show sarcomers marked by Z lines (Z). (F) Two cardiomyoctes joined together with intercalated disc (ICD) which show fascia adherence (arrow) and desmosome (arrow head). Myofibrils with Z lines (Z) and H zones (H) and regularly arranged mitochondria (m) with prominent cristae in between the miofibrils are seen. (TEM; Bar 1 μm, A, D: × 8000, B: × 4000, C: × 10000, E: × 6000, F: × 15000).

condensation of collagen fibers on their walls (**Figure 3H**).

Anti VEGF immunostained sections of control and SIL groups showed that both groups exhibited week VEGF immunoexpression by CM (**Figure 4A** and **4B**). DOX group showed strong VEGF immunoexpression by most of CM and in the wall of blood vessels (**Figure 4C**). In SIL-DOX group; Some CM exhibited mild to week VEGF immunoreactions (**Figure 4D**).

Anti-iNOS immunostained section showed faint positive iNOS immunoreaction by CM in control

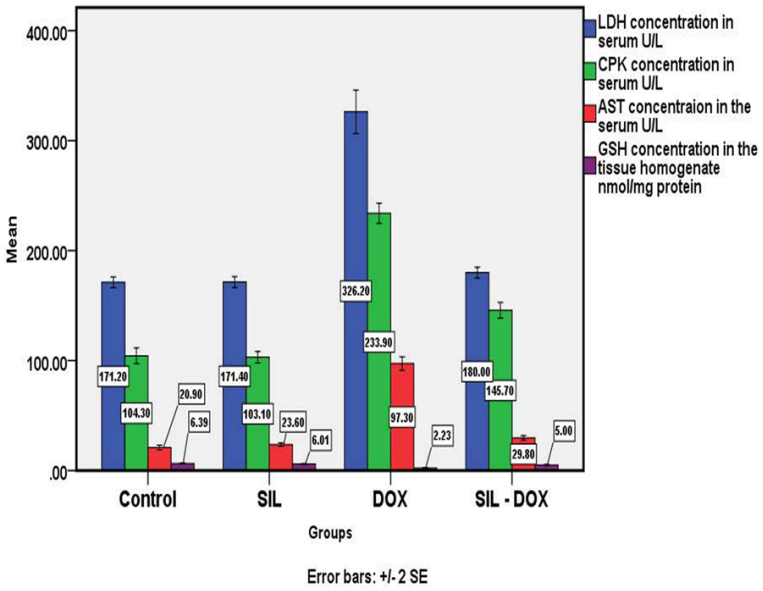

Figure 7. Clustered bars showing a highly significant increase in the mean concentration of LDH, CPK, AST and a highly significant decrease in GSH concentration in DOX groups when compared to control and SIL group. SIL-DOX group showed a highly significant decrease in the mean concentration of LDH, CPK & AST and a highly significant increase in GSH concentration when compared to DOX group. Values are expressed as mean ± standard error of mean (SE).

and SIL group (**Figure 4E** and **4F**). DOX group, showed areas of strong cytoplasmic iNOS immunoexpression by most of CM and in the wall of blood vessels (**Figure 4G**). On the other hand, in SIL-DOX group, some CM exhibited mild to weak iNOS immunoexpression (**Figure 4H**).

Anti-caspase 3 immunostained sections of control & SIL groups showed few areas of positive caspase 3 immunoactivity in CM (**Figure 4I** and **4J**). DOX group showed strong positive nuclear and cytoplasmic caspase 3 immunoexpression (**Figure 4K**), whereas SIL-DOX group exhibited mild caspase 3 immunoexpression by CM (**Figure 4L**).

Ultrastructural results

Transmission electron microscopic examination of the heart from both control and SIL group showed similar appearance. CM had regular arrangement of branching and anastomosing myofibrils that showed sarcomers marked by Z lines and H zones along their length. Rod shaped nucleus with euchromatin, intact regular sarcolemma, transverse tubules and mitochondria with prominent cristae, were also seen (**Figure 5A**, **5B**, and **5D**). CM were joined together by intact step like intercalated disc which showed fascia adherence and desmosomes (**Figure 5C** and **5E**).

In DOX group, CM appeared degenerated with irregular corrugated thick basement membrane, irregular shaped small peripheral nucleus with peripheral condensation of its chromatin and areas of loss of myofibrils. Moreover, CM with small shrunken fragmenrted nucleus, wide spaces in the cytoplasm, irregular arrangement and shape of mitochondria between remnants of myofibrils were observed. Lost intercalated disc, cytoplasmic and autophagic vacuoles were also detected. The intercellular space between cardiomyocytes was wide and contained many fibroblasts and collagen fibers (**Figure 6A-D**). On the other hand, SIL-DOX group showed CM having rode shaped nuclei with fine chromatin and regularly arranged myofibrils that showed sarcomers with Z lines and H zones. Normal shaped and regularly arranged mitochondria with prominent cristae were seen in between the myofibrils. CM were joined together with intercalated disc that showed fascia adherence and desmosome (**Figure 6E** and **6F**).

Biochemical and statistical results

No significant difference was observed in mean LDH, CPK, AST & GSH concentrations between SIL group (171.40 ± 2.486, 103.10 ± 2.588, 23.60 ± 0.718 & 6.01 ± 0.194, respectively) and control group (171.20 ± 2.471, 104.30 ± 3.565, 20.90 ± 1.069 & 6.39 ± 0.217, respectively). In DOX group; A highly significant increase in the mean concentration of LDH, CPK and AST (326.20 ± 9.908, 233.90 ± 4.581 & 97.30 ± 3.112 respectively) combined with a highly significant decrease in the mean GSH concentration (2.23 ± 0.157) were detected when compared to control group, ($P \leq 0.001$). On the other hand, SIL-DOX group showed a significant decrease in the mean LDH, CPK, AST &

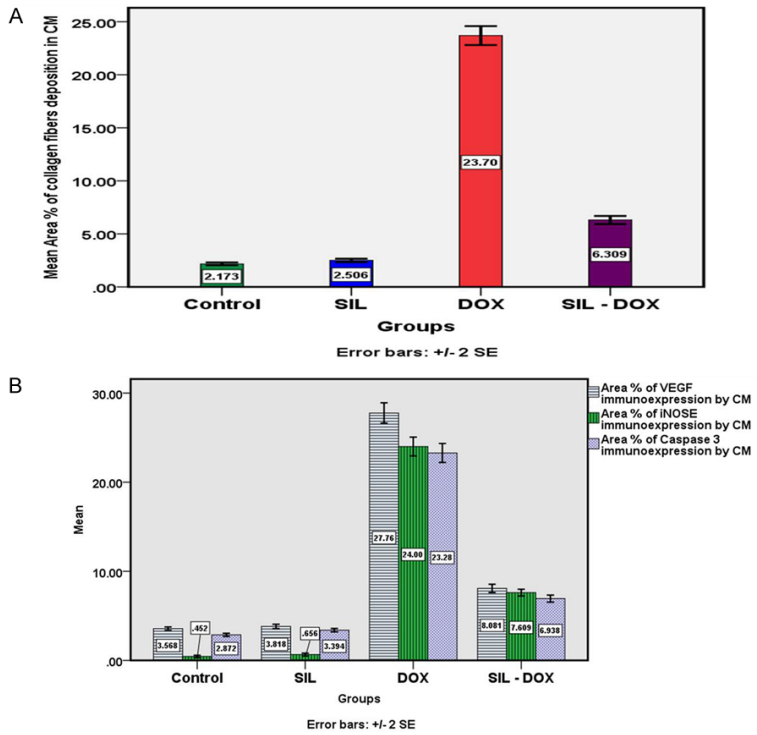

Figure 8. A: A bar graph showing the mean area% of collagen fibers in the heart tissue of control, SIL, DOX and SIL-DOX groups. B: Clustered bars representing the mean area% of VEGF, iNOS & caspase 3 immunoexpression by CM of control, SIL, DOX and SIL-DOX groups. Values are expressed as mean ± standard error of mean (SE).

GSH concentrations (180.00 ± 2.454, 145.70 ± 3.580 & 29.80 ± 1.051, respectively) and a significant increase in mean GSH concentration (5.00 ± 0.257) when compared to DOX group, $P \leq 0.001$ (**Figure 7**).

Mean area% of collagen fibers for SIL group, did not show a significant increase when compared to control group (2.17 ± 0.66 and 3.57 ± 0.09, respectively, P = 0.344). DOX group showed a highly significant increase in the mean area% of collagen (23.70 ± 0.44) when compared to control and SIL groups (($P \leq 0.001$) whereas SIL-DOX group showed a highly significant decrease (6.30 ± 0.19, $P \leq 0.001$) when compared to DOX group (**Figure 8A**).

The mean area% of VEGF, iNOS and caspase-3 immunoexpression by CM for both control (3.57 ± 0.09, 0.45 ± 0.064 & 2.87 ± 0.0.092, respectively) and SIL groups (3.81 ± 0.12, 0.65 ± 0.081 & 2.87 ± 0.0.092, respectively) didn't show any significant difference. Whereas in DOX group, the mean area% of VEGF-A, iNOS and caspase-3 immunoexpression (27.76 ± 0.57, 24.002 ± 0.53 & 23.28 ± 0.53, respectively) showed significant increase when compared to control and SIL group ($P \leq 0.001$). SIL-DOX group showed a highly significant decrease in the mean area% VEGF, iNOS and caspase-3 immunoexpression (8.08 ± 0.23, 7.60 ± 0.19 & 6.94 ± 0.20 respectively) when compared to DOX group ($P \leq 0.001$) (**Figure 8B**).

Discussion

Doxorubicin is an effective and widely used antineoplastic drug. Unfortunately, treatment with DOX is limited by cardiotoxicity shown to occur soon after beginning of therapy [26]. Several mechanisms are involved in DOX induced cardiac affection. One of the most accepted theories is the free oxygen radicals. SIL is considered to be very safe natural antioxidant and chemoprotective agent, and there are only few reports on its mechanism of action as a cardioprotective herbal derived medicine when combined with DOX.

In the current research, SIL-DOX group showed a significant decrease in the mean concentrations of LDH, CPK, AST and a significant increase in mean GSH concentration when compared to DOX group, indicating a strong cardioprotective efficacy of SIL against DOX toxicity. Serum concentrations of CPK, CK-MB and LDH, are used routinely as markers for the diagnosis of cardiac necrosis and toxicity. Compared to other organs, it was proved that the heart is more susceptible to damage by ROS due to its weak antioxidant defenses and high oxidative metabolism, therefore LDH and CK concentrations in the serum of animals treated with DOX are expected to increase over normal levels [13, 27]. Mammalian heart tissue primarily depends on glutathione peroxidase, catalase and superoxide dismutase (SOD) to protect itself from free-radical injury. Doxorubicin interferes with the activities of these antioxidant enzymes making the heart more vulnerable to

toxicity [28-30]. Accordingly, excess formation of ROS in myocardial cells and exhaustion of cellular GSH stores lead to dysregulation of antioxidant enzymes and impairment of antioxidant defenses.

The present work revealed the protective effect of silymarin against DOX-induced cardiotoxicity. This was proved by the significant decrease in serum CK, AST and LDH activities and the high increase in tissue GSH. The protective effect of SIL against elevated cardiac enzymes could be supported by the research results of other groups who pointed that DOX could cause liver and cardiac damage and consequent increase in serum transaminase activity, which could be prevented if DOX was combined with SIL [6, 28, 31]. In addition, various reported studies confirmed that SIL increases the concentration of glutathione and prevent lipid peroxidation [6, 32].

In the present study, light microscopic examination of heart tissues of DOX treated group revealed degenerated CM which had small pyknotic nuclei, vacuolated cytoplasm with areas of loss of myofibrils when compared to control and SIL groups. Marked hemorrhage, dilated and congested blood vessels were also seen between the CM. Moreover, marked increase in mean area% of collagen fibers with areas of fibrosis in between the CM and around the coronary arteries was also observed. These findings were in accordance with the work done by other groups who reported the occurrence of necrotic changes in the cardiac myocytes in the form of pyknosis, disorganization of myofibrils, loss of cross striation and marked increase in collagen fibers of the surrounding endomysium of the cardiac myocytes [6, 33, 34]. In some studies; cardiomyopathy could be diagnosed histopathologically by the disturbed orientation of cardiac muscle fibers and enlargement of their nuclei [35].

Pathological findings caused by DOX and detected in the present study are supported by reported investigations which observed marked blood cells accumulation in pericapillary space between the disordered cardiac myocytes [36]. Interference of normal oxidative metabolism caused an ischemic state followed by microvascular injury and extravasation of blood [37]. Vacuolation and degeneration of muscle fibers could be attributed to cellular injury occurring in a variety of conditions such as intoxications from chemical and metallic poisons and infectious diseases. Moreover, expansion of cytoplasmic membranous components could be caused by intracellular water and electrolytes redistribution [38, 39]. Perivascular myocardial fibrosis might be a result of myocardial ischemia that increases the stiffness of the myocardium, reducing its compliance with more deterioration [40].

The previous changes were confirmed by electron microscopy which revealed degenerated CM, irregular small peripheral nucleus with peripheral condensation of its chromatin, areas of loss of myofibrils, irregular shaped mitochondria, lost intercalated disc and cytoplasmic vacuoles. The intercellular space between CM was wide and contained fibroblasts and collagen fibers. Nearly similar changes have been previously described by [34, 41, 42]. Some investigators explained that myocardial apoptosis is a common mechanism of DOX cardiotoxicity [43-45]. Other mechanisms have been postulated, among them free radicals liberation and its direct toxic effect on cardiac muscle, disturbed mitochondrial metabolism and ability of DOX to bind to mitochondria lipids with induced lipid peroxidation [46].

In contrast, rats injected with DOX and SIL showed marked improvements in the histological changes induced by DOX. There was normal appearance of CM, preserved organization of myofibrils with minimal hemorrhage, less congestion of blood vessels and a highly significant decrease in mean area% of collagen when compared to DOX group. The above mentioned findings were also supported by the improvement of biochemical measures and elevation of GSH level. These observations were in accordance with the work done by [43-45] who proved improvement of fibrosis and modulation of the histopathological changes in cardiac tissues after administration of SIL reflecting its antifibrotic benefit. Additionally, some studies have reported the protective and antioxidant role of SIL against the animal models in which the pathogenesis was produced by oxidative stress [12, 47].

Cardioprotective effect of SIL against DOX induced oxidative stress could be attributed to its radical scavenging and cell membrane stabilizing effect. SIL significantly decreased the

damage to rat heart DNA, microsomes and protected mitochondria by triggering pro-survival cell signaling, decreasing electron leakage and reduced the activities of ROS-producing enzymes [12, 31]. The anti-inflammatory effects of SIL had been supported by the previous data of [48, 49]. They explained its inhibitory effect on the NF-κB, which is a key transcriptional factor for many genes involved in survival, regulation of cell differentiation, inflammation, immune system and apoptosis.

In this work, DOX group revealed strong VEGF, iNOS and caspase 3 immunoexpression represented statistically by highly significant increase in their mean area% compared to control group and SIL group. On the contrary, SIL-DOX group showed significant reduction in the previously mentioned parameters. This was consistent with the work done by [29, 30, 50]. Several reports suggested that DOX- can induce cardiotoxicity through ROS formation which promotes necrosis and apoptosis indicating the enhanced effect of caspase-3 activity as an important marker of apoptosis [51]. These changes could be the result of increased oxidative stress combined with low antioxidant defenses, resulting in consequent cellular and DNA damage. The decrease in the mean area% of caspase 3 immunoexpression detected in SIL-DOX group could be also explained by the decreased iNOS immunoexpression induced by SIL intake, where a direct relationship between apoptosis and iNOS over expression was observed in the present work. The anti-apoptotic effect of SIL was supported by [52] who observed that lack of iNOS can preserve cardiac function and enhance cardiac contractile and relaxation responses in iNOS knockout mice.

It was proved that iNOS can be induced in cardiac cells, which in turn result in excess production of nitric oxide (NO) [53, 54]. The induced iNOS plays a role in initiating CM death by apoptosis, myocardial remodeling, cardiac dysfunction and vascularization [54-56]. In previous researches, when the gene encoding iNOS was ablated, the expression of VEGF decreased. It is known that VEGF mediates angiogenesis in both physiologic and pathologic states and has many effects on endothelial cells related to vasodilation and permeability [54, 57, 58] In addition, iNOS regulates expression of another proinflammatory and proangiogenic enzyme, COX-2, in some systems. This explains the role of iNOS in apoptosis and angiogensis observed in DOX group. So, the decrease in expression of iNOS in SIL-DOX group might also be an evidence for the inhibitory effect of SIL on angiogenesis and apoptosis. Recently, the antiangiogenic effect of SIL was proved to be associated with decreased secretion of vascular endothelial growth factor with subsequent inhibition of capillary tube organization, arrest of growth and cell cycle, reduced invasion and migration of endothelial cells [59].

Conclusion

Based on the results of the present work, it could be concluded that silymarin can protect the heart against doxorubicin-induced cardiotoxicities, probably through the decrease of iNOS overexpression and in turn, the decrease of VEGF and caspase-3 activity and the increase in cardiac tissue GSH, suggesting its supportive role during anti-cancer treatment, particularly doxorubicin containing treatments. Therefore, silymarin may have a great potential as a novel therapeutic agent to prevent against the toxic effects induced by doxorubicin and other cardiotoxic agents. Further clinical studies are needed to determine the appropriate combination of silymarin with doxorubicin.

Acknowledgements

This study was supported by grant No. 6036/1435 from the Deanship of Taibahu University, Almadinah Almonawarah, Kingdom of Saudi Arabia.

Disclosure of conflict of interest

None.

Address correspondence to: Ghalia Mahfouz Attia, Department of Anatomy, Faculty of Medicine, Taibahu University, Al Madina Al Monawarrah, Kingdom of Saudi Arabia; Department of Histology and Cell Biology, Faculty of Medicine, Mansoura University, Al Mansoura, Egypt. Tel: 00966534397724, 0020-1225576405; E-mail: drghalia2011@gmail.com

References

[1] Jain D. Cardiotoxicity of doxorubicin and other anthracycline derivatives. J Nucl Cardiol 2000; 7: 53-62.

[2] Smith AR, Shenvi SV, Widlansky M, Suh JH, Hagen TM. Lipoic acid as a potential therapy

for chronic diseases associated with oxidative stress. Curr Med Chem 2004; 11: 1135-1164.
[3] Keizer HG, Pinedo HM, Schuurhuis GJ, Joenje H. Doxorubicin (adriamycin): a critical review of free radical-dependent mechanisms of cytotoxicity. Pharmacol Ther 1990; 47: 219-31.
[4] Myers C. The role of iron in doxorubicin-induced cardiomyopathy. Semin Oncol 1998; 25: 10-4.
[5] Boonsanit D, Kanchanapangka S, Buranakarl C. L-carnitine ameliorates doxorubicin-induced nephrotic syndrome in rats. Nephrology (Carlton) 2006; 11: 313-20.
[6] Injac R, Perse M, Cerne M, Potocnik N, Radic N, Govedarica B, Djordjevic A, Cerar A, Strukelj B. Protective effects of fullerenol C60(OH)24 against doxorubicin-induced cardiotoxicity and hepatotoxicity in rats with colorectal cancer. Biomaterials 2009; 30: 1184-1196.
[7] Mitanni I, Jain D, Joska TM, Burtness B, Zaret BL. Doxorubicin cardiotoxicity: prevention of congestive heart failure with serial cardiac function monitoring with equilibrium radionuclide angiocardiography in the current era. J Nucl Cardiol 2003; 10: 132-9.
[8] Kalyanaraman B, Joseph J, Kalivendi S, Wang S, Konorev U, Kotamraju S. Doxorubicin-induced apoptosis: implications in cardiotoxicity. Mol Cell Biochem 2002; 234-235: 119-124.
[9] Calabrese V, Cornelius C, Stella AM, Calabrese EJ. Cellular stress responses, mitostress and carnitine insufficiencies as critical determinants in aging and neurodegenerative disorders: role of hormesis and vitagenes. Neurochem Res 2010; 35: 1880-1915.
[10] Tůmová L, Tůma J, Megušar K, Doležal M. Substituted pyrazine carboxamides as biotic elicitors of flavolignan production in Silybum marianum (L.) gaertn cultures in vitro. Molecules 2010; 15: 331-340.
[11] Kroll DJ, Shaw HS, Oberlies NH. Milk thistle nomenclature: why it matters in cancer research and pharmacokinetic studies. Integr Cancer Ther 2007; 6: 110-9.
[12] Rašković A, Stilinović N, Kolarović J, Vasović V, Vukmirović S, Mikov M. The protective effects of silymarin against doxorubicin-induced cardiotoxicity and hepatotoxicity in rats. Molecules 2011; 16: 8601-8613.
[13] El-Shitany N, El-Haggar S, El-Desoky K. Silymarin prevents adriamycin-induced cardiotoxicity and nephrotoxicity in rats. Food Chem Toxicol 2008; 46: 2422-2428.
[14] Nencini C, Giorgi G, Micheli L. Protective effect of silymarin on oxidative stress in rat brain. Phytomedicine 2007; 14: 129-135.
[15] Psotova J, Chlopčikova S, Grambal F, Šimanek V, Ulrichova J. Influence of silymarin and its flavonolignans on doxorubicin- iron induced lipid peroxidation in rat heart microsomes and mitochondria in comparison with quercetin. Phytother Res 2002; 16: S63-S67.
[16] Cheung CW, Gibbons N, Johnson DW, Nicol DL. Silibinin- a promising new treatment for cancer. Anticancer Agents Med Chem 2010; 10: 186-95.
[17] Li L, Gao Y, Zhang L, Zeng J, He D, Sun Y. Silibinin inhibits cell growth and induces apoptosis by caspase activation, down-regulating survivin and blocking EGFR-ERK activation in renal cell carcinoma. Cancer Lett 2008; 272: 61-9.
[18] Li L, Zeng J, Gao Y, He D. Targeting silibinin in the antiproliferative pathway. Expert Opin Investig Drugs 2010; 19: 243-55.
[19] Ramasamy K, Agarwal R. Multi-targeted therapy of cancer by silymarin. Cancer Lett 2008; 269: 352-62.
[20] Toblli JE, Cao G, Oliveri L, Angerosa M. Comparison of oxidative stress and inflammation induced by different intravenous iron sucrose similar preparations in a rat model. Inflamm Allergy Drug Targets 2012; 11: 66-78.
[21] Tietez F. Enzymic method for quantitative determination of nanogram amounts of total and oxidized glutathione: applications to mammalian blood and other tissues. Anal Biochem 1969; 27: 502-522.
[22] Bancroft AD, Gamble M. Theory and practice of histological techniques. 6th edition. Philadelphia: Churchill Livingstone; 2008.
[23] Hsu SM, Raine L, Fanger H. Use of avidin-biotin-peroxidase complex (ABC) in immunoperoxidase techniques: a comparison between ABC and unlabeled antibody (PAP) procedures. J Histochem Cytochem 1981; 29: 577-580.
[24] Glauret AM, Lewis PR. Biological specimen preparation for transmission electron microscopy. 1st edition. London: Portland Press; 1998.
[25] Dean J, Dean AJ, Coloumbier D. Epi- Info. Software computer package was on microcomputer for epidemiology, statistics and data processing. U S A: CDC; 2004.
[26] Huang XM, Zhu WH, Kang ML. Study on the effect of doxorubicin on expressions of genes encoding myocardial sarcoplasmic reticulum Ca2+ transport proteins and the effect of taurine on myocardial protection in rabbits. J Zhejiang Univ Sci 2003; 4: 114-120.
[27] Andreadou I, Sigala F, Iliodromitis EK, Papaefthimiou M, Sigalas C, Aligiannis N, Savvari P, Gorgoulis V, Papalabros E, Kremastinos DT. Acute doxorubicin cardiotoxicity is successfully treated with the phytochemical oleuropein through suppression of oxidative and nitrosative stress. J Mol Cell Cardiol 2007; 42: 549-58.

[28] Cecen E, Dost T, Culhac N, Karul A, Ergur B, Birincioglu M. Protective effects of silymarin against doxorubicin-induced toxicity. Asian Pacific J Cancer Prev 2012; 12: 2697-2704.
[29] Chen CT, Wang ZH, Hsu CC, Lin HH, Chen JH. In vivo protective effects of diosgenin against doxorubicin-induced cardiotoxicity. Nutrients 2015; 7: 4938-4954.
[30] Panjrath GS, Patel V, Valdiviezo CI, Narula N, Narula J, Jain D. Potentiation of doxorubicin cardiotoxicity by iron loading in a rodent model. J Am Coll Cardiol 2007; 49: 2457-2464.
[31] Patel N, Joseph C, Corcoran GB, Ray SD. Silymarin modulates doxorubicin-induced oxidative stress, Bcl-xL and p53 expression while preventing apoptotic and necrotic cell death in the liver. Toxicol Appl Pharm 2010; 245: 143-152.
[32] Kolarovic J, Popovic M, Zlinská J, Trivic S, Vojnovic M. Antioxidant activities of celery and parsley juices in rats treated with doxorubicin. Molecules 2010; 15: 6193-6204.
[33] Bashandy MA, Amin SA, Seleem H. Cardiotoxic effect of chlorpromazine in adult male albino rats and the possible curcumin cardioprotection (histological, histochemical and immunohistochemical study). Journal of American Science 2012; 8: 888-898.
[34] Mohamed AA, Khalil S, Nossier S, Khalil MS. The protective role of alpha-lipoic acid against doxorubicin induced cardiotoxicity in male albino rats (a light and transmission electron microscopy study. Egypt J Histol 2009; 32: 200, 227-234.
[35] Kumar V, Abbas A, Fausto N, Aster J. Robbins and Cotran pathologic basis of diseases. 8th edition. 2010. pp. 571-577.
[36] Moustafa AMY, Shalaby AAM. Impact of trimetazidine on doxorubicin-induced acute cardiotoxicity in mice: a biochemical and electron microscopic study. Egypt J Histol 2006; 9: 125-136.
[37] Fahmy H. Effect of induced iron deficiency and iron supplementation on the myocardium of the left ventricle of post weaned male albino rat: a light and electron microscopic study. Egypt J Histol 2008; 31: 373-83.
[38] Balli E, Mete UO, Tuli A, Tap O, Kaya M. Effect of melatonin on the cardiotoxicity of doxorubicin. Histol Histopathol 2004; 19: 1101-1108.
[39] Scotti TM, Hackel DB. Coronary arteriosclerosis and myocardial hypertrophy. In: kissane JM, editor. Anderson's pathology. 8th edition. Heart Chapter 1985. pp. 1,561-570.
[40] Willenheimer R. Left ventricular remodeling and dysfunction. Can the process be prevented? Int J Cardiol 2002; 72: 143-50.
[41] Lushnikova EL, Nepomniashchich LM, Klinnikova MG, Molodykh OP. Ultrastructural manifestations of disturbances of cardiomyocyte regeneration after the doxorubicin treatment. Morfologiia 2005; 128: 81-84.
[42] Maiim MM. Potential protective effect of captopril against doxorubicin-induced cardiotoxicity in rats: light and electron microscopic study. Suez Canal Univ Med J 2005; 8: 169-178.
[43] Kim GD, Lee SE, Kim TH, Jin YH, Park YS, Park CS. Melatonin suppresses acrolein-induced IL-8 production in human pulmonary fibroblasts. Pineal Res 2012; 52: 356-364.
[44] Li PC, Chiu YW, Lin YM, Day CH, Hwang GY, Pai P, Tsai FJ, Tsai CH, Kuo YC, Chang HC, Liu JY, Huang CY. Herbal supplement ameliorates cardiac hypertrophy in rats with CCl (4)-induced liver cirrhosis. Evid Based Complement Alternat Med 2012; 139045.
[45] Shi H, Dong L, Jiang J, Zhao J, Zhao G, Dang X, Lu X, Jia M. Chlorogenic acid reduces liver inflammation and fibrosis through inhibition of toll-like receptor 4 signaling pathway. Toxicol 2013; 7: 107-14.
[46] Shalaby NM. Ultrastructural study of the toxic effect of doxorubicin on cardiac muscle. Egypt J Histol 2002; 25: 155-167.
[47] Comelli MC, Mengs U, Prosdocimi M, Schneider C. Toward the definition of the mechanism of action of silymarin: activities related to cellular protection from toxic damage induced by chemotherapy. Integr Cancer Ther 2007; 6: 120-129.
[48] Gupta SC, Tyagi AK, Deshmukh-Taskar P, Hinojosa M, Prasad S, Aggarwal BB. Downregulation of tumor necrosis factor and other proinflammatory biomarkers by polyphenols. Arch Biochem Biophys 2014; 559: 91-99.
[49] Surai PF. Silymarin as a Natural Antioxidant: an overview of the current evidence and perspectives. Antioxidants (Basel) 2015; 4: 204-247.
[50] Abdel-Wahab BA, Metwally ME. Clozapine-induced cardiotoxicity in rats: involvement of tumor necrosis factor alpha, NF-Kβ and caspase-3. Toxicology Reports1 2014; 1213-1223.
[51] Zhang YW, Shi J, Li YJ, Wei L. Cardiomyocyte death in doxorubicin-induced cardiotoxicity. Arch Immunol Ther Exp 2009; 57: 435-445.
[52] Sun Y, Carretero OA, Xu J, Rhaleb NE, Wang F, Lin C, Yang JJ, Pagano PJ, Yang XP. Lack of inducible NO synthases reduces oxidative stress and enhances cardiac response to isoproterenol in mice with deoxycorticosterone acetate-salt hypertension. Hypertension 2005; 46: 1355-61.
[53] Kleinert H, Pautz A, Linker K and Schwarz PM. Regulation of the expression of inducible nitric oxide synthase. Eur J Pharmacol 2005; 500: 255-66.

[54] Schulz R. Nitric oxide and peroxynitrite: the balance between cardioprotection and cardiotoxicity. Monaldi Arch Chest Dis 2001; 58: 155-57.
[55] Morbidelli L, Donnini S, Ziche M. Role of nitric oxide in tumor angiogenesis. Cancer Treat Res 2004; 117: 155-67.
[56] Liu MJ, Wang Z, Ju Y, Wong RN, Wu QY. Diosgenin induces cell cycle arrest and apoptosis in human leukemia K562 cells with the disruption of Ca2+ homeostasis. Cancer Chemother Pharmacol 2005; 55: 79-90.
[57] Kisley LR, Barrett BS, Bauer AK, Dwyer-Nield LD, Barthel B, Meyer AM. Genetic ablation of inducible nitric oxide synthase decreases mouse lung tumorigenesis. Cancer Res 2002; 62: 6850-6.
[58] Melly LF, Marsano A, Frobert A, Boccardo S, Helmrich U, Heberer M, Eckstein FS, Carrel TB, Giroud MN, Tevaearai HT, Banfi A. Controlled angiogenesis in the heart by cell-based expression of specific vascular endothelial growth factor levels. Hum Gene Ther Methods 2012; 23: 346-356.
[59] Singh RP, Dhanalakshmi S, Agarwal C, Agarwal R. Silibinin strongly inhibits growth and survival of human endothelial cells via cell cycle arrest and downregulation of survivin, Akt and NF-kappaB: implications for angioprevention and antiangiogenic therapy. Oncogene 2005; 24: 1188-1202.